Oblique-incidence far-infrared reflectivity study of the uniaxial antiferromagnet FeF$_2$

Kamsul Abraha

Department of Physics, University of Essex, Colchester CO4 3SQ, United Kingdom
and Jurusan Fisika, Universitas Gadjah Mada, Yogyakarta 55281, Indonesia

D. E. Brown, T. Dumelow, and T. J. Parker

Department of Physics, University of Essex, Colchester CO4 3SQ, United Kingdom

D. R. Tilley

Department of Physics, University of Essex, Colchester CO4 3SQ, United Kingdom
and School of Physics, Universiti Sains Malaysia, 11800 USM Penang, Malaysia

Theoretical and experimental results are presented for high-resolution frequency scans of 45° oblique-incidence far-infrared reflectivity spectra of FeF$_2$ in the vicinity of the antiferromagnetic resonance frequency. The magnetic field is vertical and the plane of incidence horizontal. Calculations are presented and illustrated numerically for an arbitrary angle θ between the crystal c axis and the magnetic field H_0. The main point of principle is that the equilibrium spin configuration and therefore the magnetic susceptibility depend on θ. The reflectivity R is nonreciprocal, i.e., $R(-H_0) \neq R(H_0)$. For $\theta = 0°$ magnetic features are seen only in s polarization (E field vertical), but otherwise they are seen in both polarizations. Except for $\theta = 0°$ and 90° weak s to p and p to s reflections are predicted. We discuss the instrumental developments required for the high resolution that is necessary for this spectroscopy. Experimental results for $\theta = 45°$ are presented ($\theta = 0°$ and 90° are in a previous publication). The whole range of spectra, including the s to p and p to s reflections, are accounted for with the same set of parameters as were used previously to fit the $\theta = 0°$ and 90° results.

I. INTRODUCTION

In order of increasing wavelength the spin-wave excitation spectrum of magnetic systems can usually be divided into exchange, dipolar (magnetostatic), and retarded (electromagnetic) regions. The first two have been extensively studied both experimentally and theoretically. However, despite a substantial theoretical literature[1,2] there have been relatively few experimental studies of the retarded region. We have recently developed[3] a high-resolution Fourier-transform far-infrared (FIR) spectrometer suitable for such studies in the frequency range from 10 to 500 cm^{-1}. This includes many antiferromagnetic resonance frequencies as well as the exchange and higher resonances of ferrimagnets. The retarded regions associated with most of these resonances are up to now almost totally unexplored. In addition to the early measurement of antiferromagnetic resonance[4] previous work on uniaxial antiferromagnets includes zero-field, low-resolution frequency-scan reflectivity measurements on FeF$_2$ and CoF$_2$,[5,6] a magnetic-field scan of reflectivity off MnF$_2$ (Ref. 7) and a study of transmission through thin (15–800 μm) samples.[8] This latter study, like Ref. 7, used a magnetic-field scan with a fixed-frequency (FIR laser) source. The most substantial experimental work in recent years on magnetic resonances in this spectral region has been a sustained study of the rare-earth orthoferrites.[9,10] In a long series of papers, spectral features due to electronic transitions in the rare-earth ions as well as

the ferromagnetic and antiferromagnetic resonances were identified. However, the experimental geometry was restricted to normal incidence and little of the work involved applied magnetic fields.

Our first investigation was of FeF$_2$, which has a resonance frequency at the convenient value of around 50 cm^{-1}. It has the tetragonal rutile structure[11] with sublattice orderings along the c axis. Much of the theoretical literature is concerned with surface magnetic polaritons and the associated spectroscopy of attenuated total reflection (ATR). However, our experience of similar spectroscopy on semiconductors[12] is that the simpler technique of oblique-incidence reflectivity yields a considerable amount of useful information. We, therefore, used this technique with an angle of incidence $\phi = 45°$ although we plan to introduce ATR later.

Both reflectivity and the propagation of surface polaritons are governed by the frequency-dependent magnetic permeability tensor $\overleftrightarrow{\mu}(\omega)$. This takes a gyrotropic form with nonvanishing off-diagonal elements that are proportional to the magnetic field H_0.[13] Most calculations of $\overleftrightarrow{\mu}(\omega)$ assume that the c axis is along $\mathbf{H}_0$. An important point of principle is that if the c axis is turned away from $\mathbf{H}_0$ the Zeeman energy, tending to align all spins along $\mathbf{H}_0$, competes with the exchange energy, which favors antiparallel alignment of the sublattice moments. Consequently for a general angle θ between the c axis and $\mathbf{H}_0$ the sublattice moments are not exactly antiparallel. Since the equilibrium configuration depends on θ, $\overleftrightarrow{\mu}(\omega)$ also de-

pends on θ. Fortunately the very laborious calculations required to find $\overleftrightarrow{\mu}(\omega)$ for general θ have already been carried out by Almeida and Mills.[14] One important consequence of the form of $\overleftrightarrow{\mu}(\omega)$, even for $\theta=0$, is that the reflectivity R is nonreciprocal, $R(-H_0)\neq R(H_0)$. A full discussion of nonreciprocity is given in Ref. 1.

A brief report on our experimental results, together with theoretical comparisons, for the simple geometries of c axis along and transverse to H_0 ($\theta=0$ and $90°$) has already appeared.[15] The reflectivity has a sharply defined feature at the position of the antiferromagnetic (AF) resonances. For $\theta=0$ in zero field we measure the AF resonance frequency and linewidth from 4.2 up to 30 K, i.e., about half the Néel temperature T_N. As is well known from earlier AF resonance experiments[4,8,16] the frequency decreases and the linewidth increases sharply as the temperature increases. The values we obtained for the linewidth[15] are very close to those obtained by Sanders et al.[8] It may be noted also that Rezende and Hone[17] carried out a Green's function calculation of the temperature dependence of the magnon dispersion and related quantities arising from magnon-magnon interactions and this method could be applied to a calculation of the temperature dependence of the dynamic susceptibility. Returning to our previous experimental results, application of a field for $\theta=0$ results in a Zeeman splitting of the resonance line; both this splitting and the predicted nonreciprocity of the reflectivity are seen very clearly in the spectra. All the $\theta=0$ spectra are taken in s polarization (E field transverse to the plane of incidence), since there is no coupling to the resonant elements of $\overleftrightarrow{\mu}(\omega)$ in p polarization. For $\theta=90°$ the theoretical expression for $\overleftrightarrow{\mu}(\omega)$ (Ref. 14) shows that resonances at different frequencies should be seen in the two polarizations. This indeed proved to be the case.

In this paper we give a fuller account of the theory (Sec. II) and the instrumentation (Sec. III) than have appeared previously. In addition to the $\theta=0°$ and $90°$ results already reported,[15] we have measured spectra for $\theta=45°$; these are presented and discussed in Sec. IV. Conclusions are given in Sec. V.

II. THEORY

Following Almeida and Mills[14] we show in Fig. 1 a schematic diagram of the sublattice orientations for a general angle θ between the magnetic field and the easy axis. The Hamiltonian is written as a sum of exchange with field H_E, single-ion anisotropy DS_z^2, Zeeman energy in the static field H_0 and linear coupling to the rf field $h\exp(-i\Omega t)$. With the last term omitted the equations for equilibrium lead to coupled nonlinear equations for the angles α_a and α_b defined in Fig. 1; the numerical solution of these is straightforward. The linear response of the spin system to h gives the elements of the rf susceptibility tensor $\overleftrightarrow{\chi}$ in the usual way. The full expression[14] is too lengthy to be quoted here. For general θ all components of $\overleftrightarrow{\chi}$ are nonzero and although it is not obvious from the formulas numerical evaluation of the elements of $\overleftrightarrow{\chi}$ shows that it is Hermitian. It should be noted that the formulas in Ref. 14 contain a trivial misprint: γ
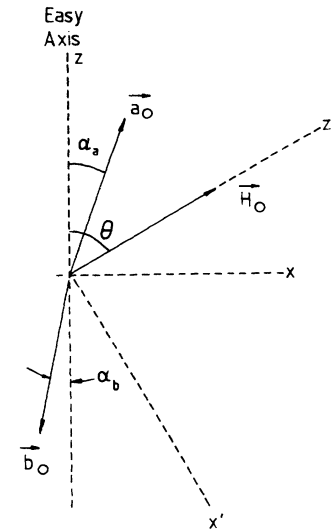

FIG. 1. Sublattice orientations for general angle θ between the applied field H_0 and the easy axis. A further explanation of this figure is given in Sec. II of the text.

should be replaced by γM_s throughout. The form of $\overleftrightarrow{\chi}$ for the special case $\theta=0°$ is well known[13] and the form for $\theta=90°$ is quoted in Ref. 14. For calculation of reflectivity it is necessary to include damping, and we do this by the replacement $\Omega\rightarrow\Omega+i\Gamma$. In Ref. 14 $\overleftrightarrow{\chi}$ is given for axes with z along the easy direction. In our equipment, however, H_0 remains vertical and the crystal is rotated through angle θ so the first stage of our calculation is a tensor rotation of $\overleftrightarrow{\chi}$ to the $x'z'$ axes defined in Fig. 1. Our subsequent calculations are in terms of the permeability $\overleftrightarrow{\mu}=1+\overleftrightarrow{\chi}$.

The derivation of the expressions for the reflectivity involves a sequence of steps familiar from ordinary optics. The notation is defined in Fig. 2. Since for the general
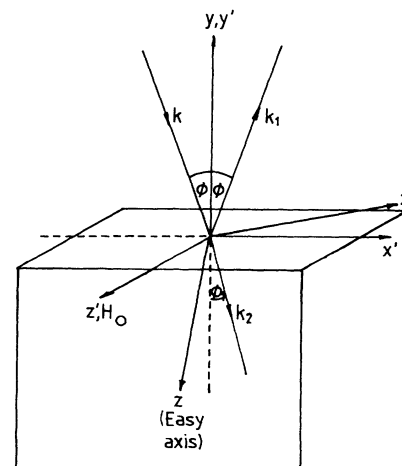

FIG. 2. Notation for reflectivity calculation. Axes (xz) and $(x'z')$ are the same as in Fig. 1; y and y' coincide and are the normal to the surface. Angles of incidence and refraction are ϕ and ϕ_1. Incident, reflected and refracted waves have wave vectors k, k_1, and k_2.

case $\bar{\mu}$ has no zero elements the FeF_2 crystal is birefringent with two possible values of wave number k_2 and angle of refraction ϕ_1. For each wave these are related by Snell's Law (conservation of parallel wave vector component):

$$k_2\sin\phi_1 = k\sin\phi . \tag{1}$$

The electromagnetic wave equation in the crystal leads to

$$k_2^4 - Ak_2^2 - D = 0 , \tag{2}$$

where

$$A = [(\mu_{y'y'} - \mu_{x'x'})k^2\sin^2\phi$$
$$+ q^2(\mu_{x'x'}\mu_{y'y'} + \mu_{y'y'}\mu_{z'z'}$$
$$- \mu_{x'y'}\mu_{y'x'} - \mu_{y'z'}\mu_{z'y'})]/\mu_{y'y'} \tag{3}$$

and

$$D = [q^2(\mu_{x'x'}\mu_{z'z'} + \mu_{y'z'}\mu_{z'y'} - \mu_{x'z'}\mu_{z'x'}$$
$$- \mu_{y'y'}\mu_{z'z'})k^2\sin^2\phi + C]/\mu_{y'y'} , \tag{4}$$

$$C = q^4(C_1 + C_2 + C_3) \tag{5}$$

with $q^2 = \epsilon\omega^2/c^2$, where ϵ is the dielectric constant of the crystal and

$$C_1 = \mu_{x'x'}(\mu_{y'z'}\mu_{z'y'} - \mu_{y'y'}\mu_{z'z'}) , \tag{6}$$

$$C_2 = \mu_{x'y'}(\mu_{y'x'}\mu_{z'z'} - \mu_{y'z'}\mu_{z'x'}) , \tag{7}$$

$$C_3 = \mu_{x'z'}(\mu_{y'y'}\mu_{z'x'} - \mu_{y'x'}\mu_{z'y'}) . \tag{8}$$

The two values of k_2 are given by (2).

Consider first an s polarized incident beam, $\mathbf{E} = (0,0,E_0)$. Because there are two refracted beams, there are also two reflected beams, one s polarized and one p polarized, with E fields $(0,0,R_sE_0)$ and $(S_sE_0, -S_sE_0\sin\phi/\cos\phi, 0)$, respectively. The electromagnetic boundary conditions lead to four linear equations in the reflection coefficients R_s and S_s and two transmission coefficients T_+ and T_-. Solution of these gives expressions

$$R_s = \frac{\sigma_-(\lambda_-k + \rho_-\cos\phi)(\sigma_+k\cos\phi + \rho_+) - \sigma_+(\lambda_+k + \rho_+\cos\phi)(\sigma_-k\cos\phi + \rho_-)}{\sigma_-(\lambda_-k + \rho_-\cos\phi)(\sigma_+k\cos\phi - \rho_+) - \sigma_+(\lambda_+k + \rho_+\cos\phi)(\sigma_-k\cos\phi - \rho_-)} \tag{9}$$

for the s-to-s reflection and

$$S_s = \frac{2\sigma_+\sigma_-(\lambda_+\rho_- - \lambda_-\rho_+)k\cos^2\phi}{\sigma_-(\lambda_-k + \rho_-\cos\phi)(\sigma_+k\cos\phi - \rho_+) - \sigma_+(\lambda_+k + \rho_+\cos\phi)(\sigma_-k\cos\phi - \rho_-)} \tag{10}$$

for the s-to-p reflection. The quantities appearing are

$$\sigma_\pm = \frac{q^2(k_2^{\pm 2} - k^2\sin^2\phi)^{1/2}[\mu_{z'y'}(k_2^{\pm 2} - k^2\sin^2\phi)^{1/2} - i\mu_{z'x'}k\sin\phi] + q^4(\mu_{x'y'}\mu_{z'x'} - \mu_{x'x'}\mu_{z'y'})}{(k_2^{\pm 2} - q^2\mu_{z'z'})[q^2\mu_{x'y'} - i(k_2^{\pm 2} - k^2\sin^2\phi)^{1/2}k\sin\phi] + q^4\mu_{x'z'}\mu_{z'y'}} , \tag{11}$$

$$\rho_\pm = \frac{q^2\lambda_\pm}{(k_2^{\pm 2} - k^2\sin^2\phi)^{1/2}} , \tag{12}$$

$$\lambda_\pm = \frac{q^2\mu_{z'y'}\sigma_\pm(k_2^{\pm 2} - k^2\sin^2\phi)^{1/2}}{q^2[i\mu_{z'x'}k\sin\phi - \mu_{z'y'}(k_2^{\pm 2} - k^2\sin^2\phi)^{1/2}] - i\sigma_\pm(k_2^{\pm 2} - q^2\mu_{z'z'})k\sin\phi} . \tag{13}$$

Similar calculations for incident p polarization give

$$R_p = T_p^+ + T_p^- - 1 \tag{14}$$

for p to p reflection and

$$S_p = T_p^+/\lambda_+ + T_p^-/\lambda_- \tag{15}$$

for p-to-s reflection. T_p^+ and T_p^-, which are in fact the two transmission coefficients, are given by

$$T_p^\pm = \frac{\pm 2k\lambda_\pm^2\sigma_\pm(\sigma_\pm\lambda_\pm k\cos\phi - \rho_\mp\lambda_\mp)}{\lambda_+\sigma_+(\lambda_+k + \rho_+\cos\phi)(\sigma_-\lambda_-k\cos\phi - \rho_-\lambda_-) - \lambda_-\sigma_-(\lambda_-k + \rho_-\cos\phi)(\sigma_+\lambda_+k\cos\phi - \rho_+\lambda_+)} . \tag{16}$$

The special cases of these formulae for $\theta = 0°$ and $90°$ were used previously[15] for comparison with the experimental spectra. For these high-symmetry orientations the "cross reflections" (s to p and p to s) vanish.

The appearance of a term $k\sin\phi$ in λ_+ and λ_- and elsewhere is an indication that the above expressions imply nonreciprocal reflectivity. In either polarization the behavior of all the reflection coefficients under sign

changes of θ, ϕ, and H_0 may be summarized as follows (U stands for any one of R_s, R_p, S_s, and S_p):

$$U(-\theta) = U(\theta) ,$$ (17)

$$U(-H_0) \neq U(H_0) ,$$ (18)

$$U(-\phi) \neq U(\phi) ,$$ (19)

$$U(-H_0, -\phi) = U(H_0, \phi) .$$ (20)

This last result implies that reversing H_0 is equivalent to reversing the angle of incidence ϕ, which is consistent with a discussion of nonreciprocity based on symmetry.[18]

We now give computed reflectivity curves to illustrate some numerical implications of the reflectivity formulae for FeF$_2$. First we recall from Ref. 15 that for $\theta = 0°$ the magnetic features are seen only in s polarization and there is no s-to-p reflection. For $\theta = 90°$ resonances at two different frequencies are seen in both s and p polarization but there is no s-to-p or p-to-s reflection. Figure 3 shows computed reflectivities (square moduli of the amplitude expressions given above) for $H_0 = 3$ T and a range of angles θ from $0°$ to $90°$. The magnetic parameters (resonance frequency $\omega_{AF}/2\pi c = 52.45$ cm^{-1}, damping

$\Gamma/2\pi c = 0.05$ cm^{-1} and dielectric constant $\varepsilon = 5.5$) are the same as gave the best fit to the $\theta = 0°$ and $90°$ spectra at 4.2 K.[15] These parameters are only slightly different from those used by Sanders et $al.$[8] in their transmission studies of FeF$_2$ crystals.

The nature and field dependences of the resonances for $\theta = 0°$ and $90°$ are very different. The $\theta = 0°$ s-to-s spectrum, Fig. 3(a), shows a simple Zeeman splitting together with a marked asymmetry between the upshifted and downshifted features. For $\theta = 90°$, however, there is no Zeeman splitting but the spectra show a weak quadratic dependence on H_0, numerically $\delta\omega_r/2\pi c = 7.2 \times 10^{-3} H_0^2$, where H_0 is in Tesla and the frequency shift is in cm^{-1}. These predictions, derived from the Almeida-Mills susceptibility tensor, were confirmed experimentally in Ref. 15. The evolution of the s-to-s spectrum as θ is changed is illustrated with the computed spectra of Fig. 3(a).

The p-to-p spectra for the same values of θ are shown in Fig. 3(c). As mentioned, there is no coupling to the magnetic resonances for $\theta = 0°$ and as θ is increased a Zeeman split spectrum develops and strengthens. The frequency splitting decreases as θ increases until at $\theta = 90°$ a single strong feature is seen. This has the weak
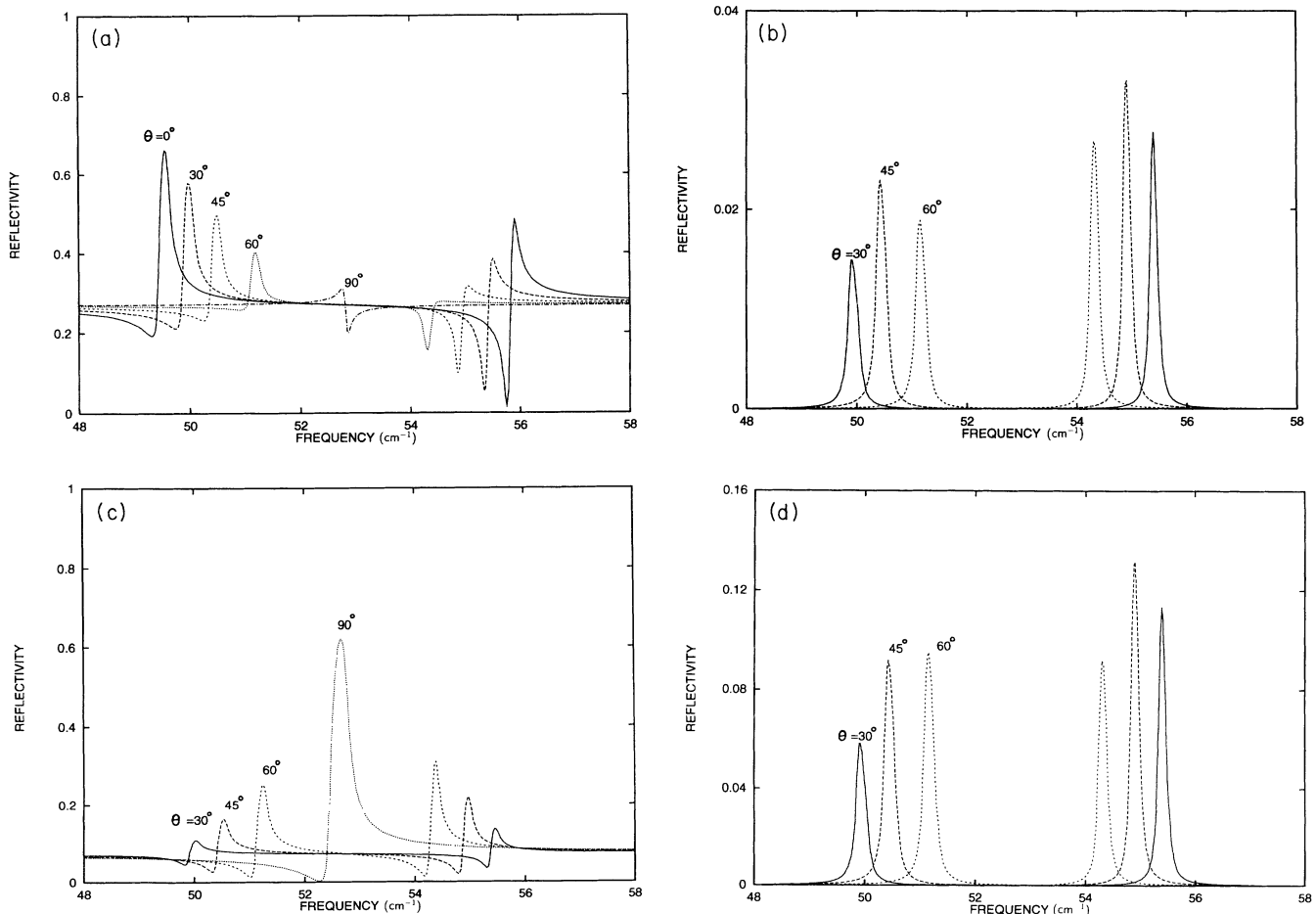

FIG. 3. Computed spectra for a range of crystal orientations θ in a field $H_0 = +3T$ with parameters appropriate to FeF$_2$ at 4.2 K. Polarization combinations are (a) s to s, (b) s to p, (c) p to p, and (d) p to s.

quadratic dependence, verified experimentally in Ref. 15, $\delta\omega_r/2\pi c = -1.6 \times 10^{-3} H_0^2$.

A distinctive characteristic of the reflectivities away from the high-symmetry directions $\theta = 0°$ and $90°$ is the appearance of weak s-to-p and p-to-s reflections as given by (7) and (12). Curves to illustrate these are shown in Figs. 3(b) and 3(d); as might be expected these cross reflections are a maximum around $\theta = 45°$. It will be seen that the p-to-s reflections are stronger than the s-to-p ones by a factor of about 4. We have carried out a detailed experimental study of all the spectra for $\theta = 45°$ and the results are presented in Sec. IV.

III. INSTRUMENTATION

An NPL (National Physical Laboratory) far-infrared cube interferometer[19] has been modified for this work[3] by adding a hydraulically controlled moving mirror arm with a scan length of 1 m and a single mode He-Ne laser to monitor the optical path difference so that measurements can be made with a nominal resolution of 10^{-2} cm^{-1}. The specimen is located between the poles of a 7-T magnet. The instrument is shown schematically in Fig. 4, and the main features are described below.

The moving mirror is mounted on a high-precision slide and scanned continuously at a constant speed of ~ 16 μm/s. In the fixed arm of the interferometer the end mirror is vibrated at ~ 167 Hz in a direction normal to the incident beam to provide phase modulation[20,21] for the infrared beam. For the present work the amplitude of vibration is set at ~ 50 μm to provide optimum modulation of the infrared beam at frequencies near 50 cm^{-1}, the antiferromagnetic resonance frequency of FeF$_2$, and the infrared radiation is detected using a liquid-He-cooled Si bolometer and a lock-in amplifier system.

The He-Ne laser beam passes along the optical axis of the instrument and the laser fringes are detected using a photodiode placed immediately after the beam divider. The laser beam is reflected from a small fixed mirror to a fixed, but adjustable, side mirror, so that it is not incident on the vibrating mirror. However, the laser fringes are modulated (at ~ 500 Hz) by the continuous variation of

the optical path difference resulting from the motion of the moving mirror and, by using a voltage discriminator, they are counted and used to measure the optical path difference between the two beams and determine the sampling intervals for the infrared beam. Cross talk in the infrared channel due to modulation from the continuous scan of the moving mirror is rejected, since the slower modulation frequency (~ 1 Hz) is rejected by the lock-in amplifier. Interferograms are coadded until a satisfactory signal-to-noise ratio is obtained.

In this interferometer the advantages of phase sensitive detection of the infrared beam and high-precision optical sampling of the interferogram are achieved simultaneously. A major improvement in the signal-to-noise ratio, S/N, is obtained due to the large reduction in the noise bandwidth by the phase sensitive detector; with a time constant of 100 ms, as used in this work, the improvement is ~ 45 dB. A further improvement in S/N, as required, is then achieved by coadding interferograms. Consequently, data can be obtained more rapidly than by using the scanning mirror to modulate the far-infrared beam and coadding interferograms.

The far-infrared output beam from the beam divider is focussed on to the sample, which is located between the poles of a 7-T magnet in a liquid-He cryostat, and the beam reflected from the sample is subsequently focussed on to the bolometer operating at 4.2 K. A Spectromag SM6 magnet and cryostat from Oxford Instruments Ltd., with the field vertical, are used for this work and the plane of incidence is horizontal.

The output beam from the interferometer is strongly s polarized in the vertical plane due to the Fresnel reflectivity of the Mylar beam divider, so that measurements on the specimen can be made straightforwardly in s polarization. It is not possible, however, to make p-polarized measurements with an acceptable signal-to-noise ratio in a reasonable time using the direct p-polarized output component from the beam divider (the ratio of the intensities of the s and p components is $s:p \sim 6:1$); neither is it possible to reorient the cryostat and magnet for such measurements. Instead, the s-polarized beam from the beam divider is utilized, and a
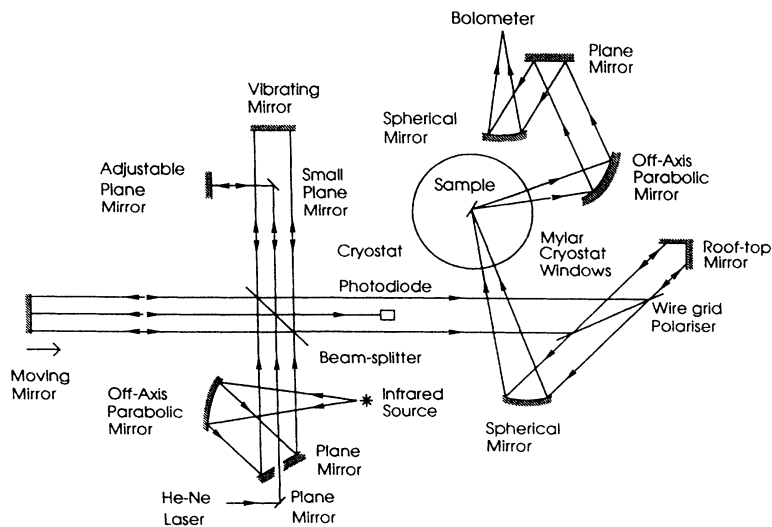

FIG. 4. Schematic diagram of the Michelson interferometer set up for p-polarized measurements.

combination of a roof-top mirror and free-standing wire grid polarizer is used[22] to rotate the plane of polarization by 90° before the beam enters the cryostat. This is satisfactory for most measurements, but, as will be seen later, the efficiency of a wire grid polarizer is only about 98%,

at the wavelengths of the present work,[22] and this leads to significant polarization cross talk in some of the measurements.

IV. EXPERIMENTAL SPECTRA

In this section we present theoretical and experimental results for the reflectivity at angle of incidence $\phi=45°$ for
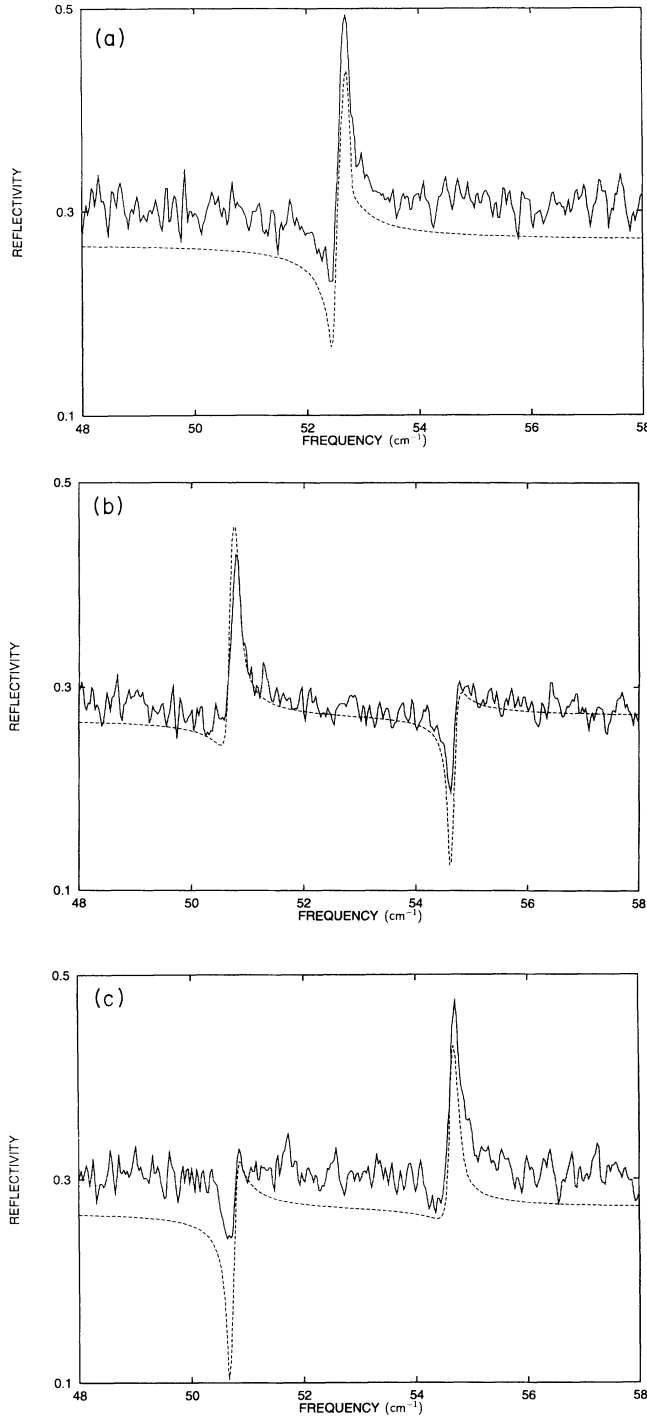
FIG. 5. Experimental (solid lines) and theoretical s-to-s (dashed lines) reflectivities at 4.2 K for $\theta=45°$ and angle of incidence 45°. Experimental resolution 0.06 cm^{-1}. The linewidths are instrumental: (a) $H_0=0$ T, (b) $H_0=+3$ T, and (c) $H_0=-3$ T.
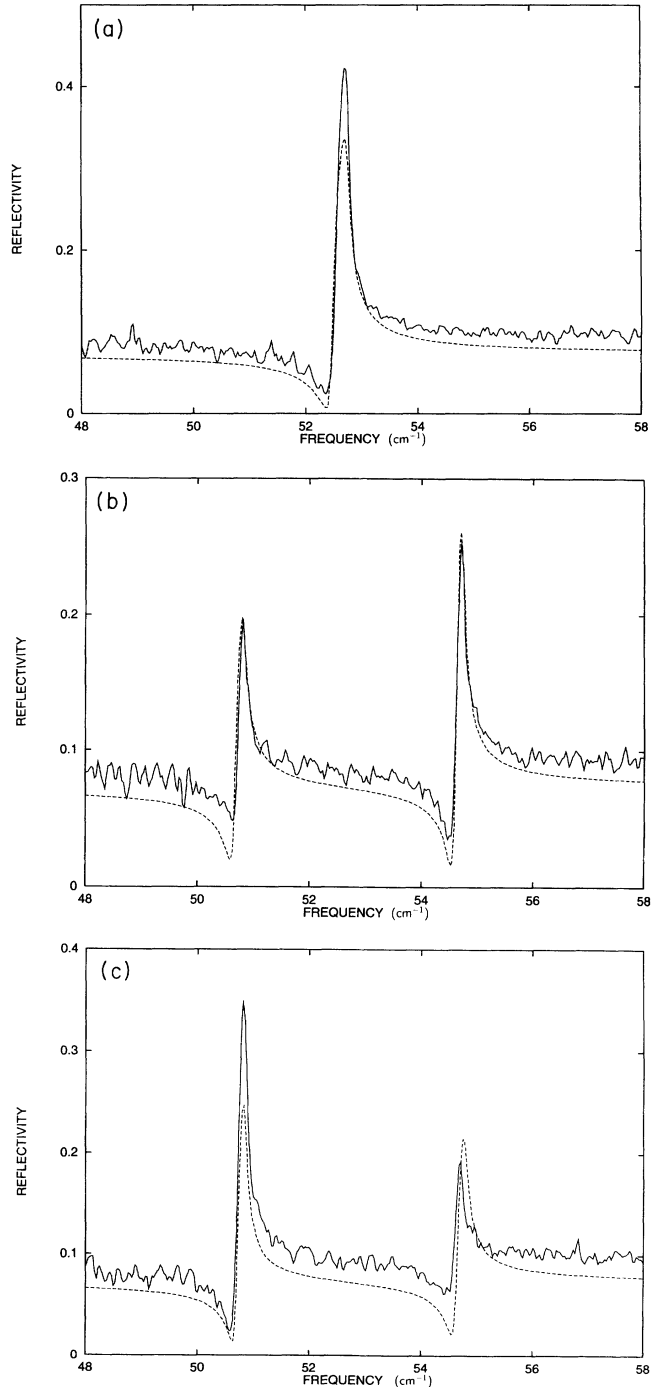
FIG. 6. Experimental (solid lines) and theoretical (dashed lines) p-to-p reflectivities at 4.2 K for $\theta=45°$ and angle of incidence 45°. Experimental resolution 0.06 cm^{-1}. The linewidths are instrumental: (a) $H_0=0$ T, (b) $H_0=+3$ T, and (c) $H_0=-3$ T.

the case when the angle θ between the c axis and the field is 45°; results for $\theta = 0°$ and $\theta = 90°$ have been published previously.[15] All the spectra shown were taken at 4.2 K. The theoretical curves are calculated from the formulas of Sec. II with the same numerical parameters as were used for the $\theta = 0°$ and 90° spectra.
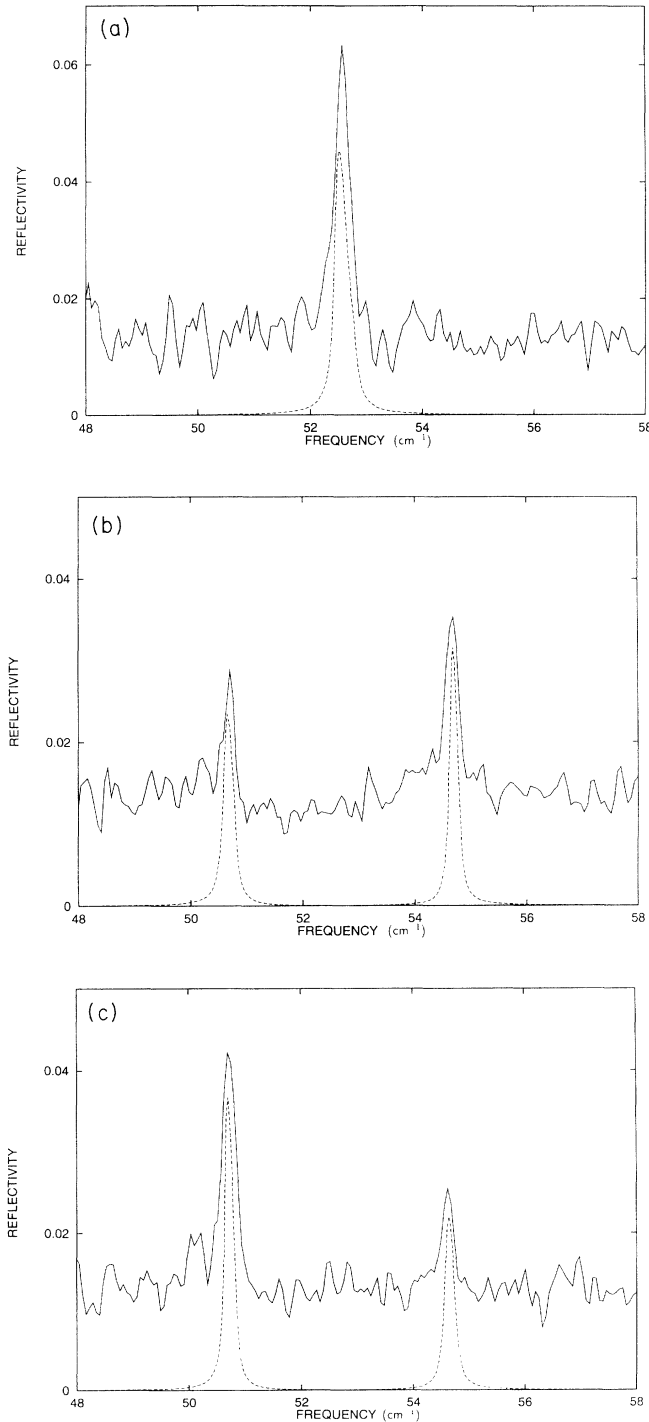
The reflectivity for s-to-s polarization is shown in Fig. 5. In zero field it has a similar asymmetric shape to that seen for $\theta = 0°$. As in the case of the $\theta = 0°$ spectrum, application of a magnetic field produces a Zeeman splitting although, as Fig. 3 shows, the splitting here is smaller. The nonreciprocity is evident in the different forms of the
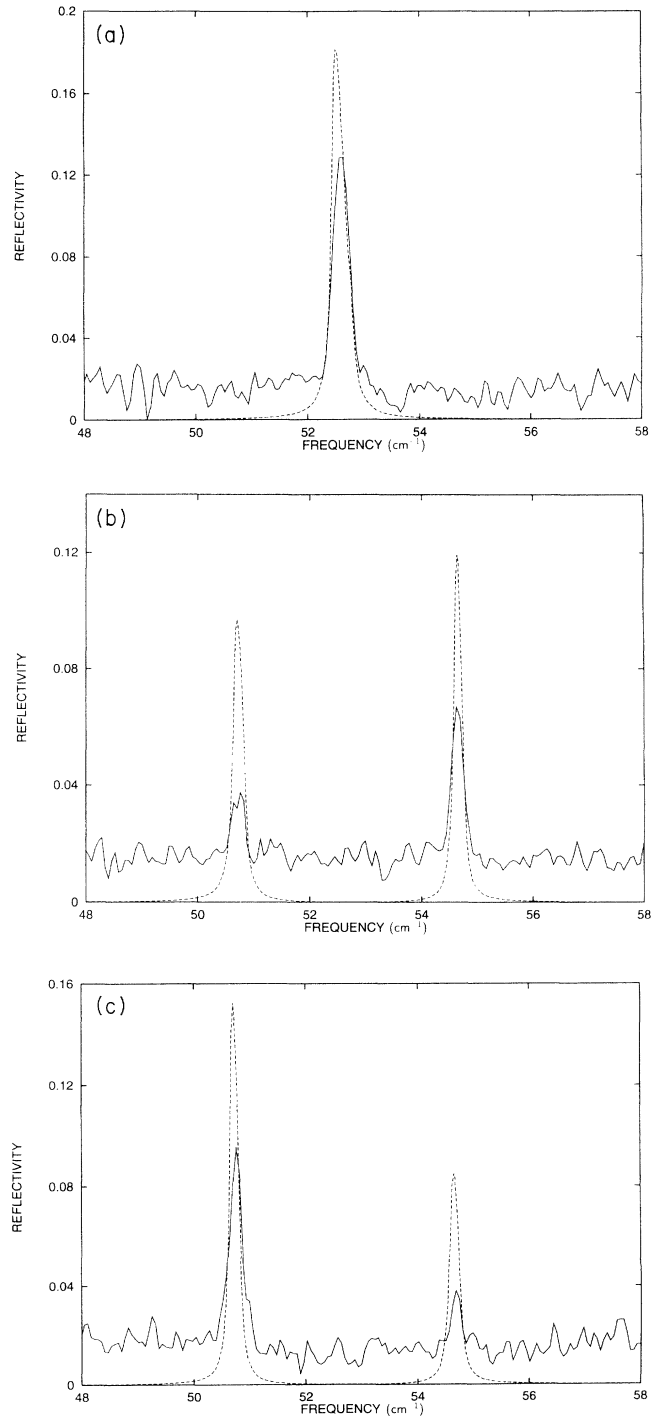
FIG. 7. Experimental (solid lines) and theoretical (dashed lines) s to p reflectivities at 4.2 K for $\theta = 45°$ and angle of incidence 45°. Experimental resolution 0.06 cm^{-1}. The linewidths are instrumental. (a) $H_0 = 0$ T, (b) $H_0 = +3$ T, (c) $H_0 = -3$ T.

FIG. 8. Experimental (solid lines) and theoretical (dashed lines) p-to-s reflectivities at 4.2 K for $\theta = 45°$ and angle of incidence 45°. Experimental resolution 0.06 cm^{-1}. The linewidths are instrumental: (a) $H_0 = 0$ T, (b) $H_0 = 3$ T, and (c) $H_0 = -3$ T.

spectra for ±3 T.

Figure 6 shows the corresponding p-to-p reflectivity curves. The 0 T curve is similar in form to that found for $\theta=90°$; there is no $\theta=0°$ reflectivity for comparison. For ±3 T, however, the present curves show a Zeeman splitting, whereas there is no splitting in the $\theta=90°$ reflectivity, only the weak shift, quadratic in the field, mentioned previously. Associated with the Zeeman splitting is a pronounced nonreciprocity between the ±3 T curves.

In Sec. II expressions were derived for the weak s-to-p and p-to-s reflectivities predicted away from $\theta=0°$ or 90° and some illustrations of computed curves were given in Figs. 3(b) and 3(d). Despite the weakness of these reflections we have succeeded in measuring them at $\theta=45°$. Figures 7 and 8 show s-to-p and p-to-s curves, respectively, in fields of ±3 T. All the curves show a weak nonzero background outside of the magnetic resonance. The background levels are due to leakage through the grid polarizer of the unwanted incident polarization, and the magnitude is in quantitative agreement with predictions based on the exact theory of grid polarizers.[22] We have chosen not to substract off this background from the experimental curves.

For the weak signals in Figs. 7 and 8 we do not have very good agreement in all cases between the magnitudes of the experimental and theoretical curves. However, there is good agreement over all the qualitative features. The general scales do agree, and, in particular, the p-to-s reflectivity is significantly stronger than the s-to-p. The expected nonreciprocity is also clear.

V. CONCLUSIONS

In this and our previous paper[15] we have presented an extensive study of far-infrared reflectivity off the uniaxial antiferromagnet FeF_2. Although related work[4,8] on antiferromagnetic resonance in FeF_2 dates back as long as 30 years, we have been able to find a number of new effects by working in oblique incidence. The evidence for nonreciprocal reflection in the $\theta=0°$ spectra adds substantially to that previously published.[7] As far as we are aware, there have been no previous publications of spectra away from $\theta=0°$. Our results at $\theta=90°$ (Ref. 15) and 45° (Sec. IV) provide a detailed test of the modification of the magnetic susceptibility tensor $\overleftrightarrow{\chi}$ resulting from the reorientation of the sublattice moments. Our reflectivity calculations (Sec. II) together with Almedia and Mills's formulas[14] for $\overleftrightarrow{\chi}$ leads to theoretical curves that agree in all particulars with the experimental spectra. The main points

in addition to the general nonreciprocity are as follows. Although there is no coupling to the magnetic resonance in p polarization at $\theta=0°$, coupling does occur for $\theta\neq0°$. For $\theta=90°$ resonances occur at different frequencies in s and p polarization. These are not Zeeman split by an applied field; instead they show only small shifts quadratic in H_0 and of opposite sign. For values of θ intermediate between 0° and 90° both s and p spectra are Zeeman split, although the extent of the splitting is smaller than that for s polarization at $\theta=0°$. For these intermediate values the symmetry is sufficiently low that weak s-to-p and p-to-s reflections are seen.

Despite the antiquity of studies on uniaxial antiferromagnets, we believe that there is still scope for further work. Much of the theory that has been done[1,2] is concerned with surface antiferromagnetic polaritons and particularly their nonreciprocal propagation. However, there has been no experimental work. We plan to rectify this by the development of an ATR stage. A notable omission in our work to date is the investigation of spectra in nonzero field at higher temperatures than 4.2 K. Almeida has pointed out recently[23] that even for $\theta=0°$ the calculation of $\overleftrightarrow{\chi}$ at nonzero temperature is a subtler matter than at zero temperature. The decrease with temperature of the moment of the sublattice aligned with the field is slower than that of the other sublattice. Consequently care is needed over the definitions of the exchange and anisotropy fields and therefore of the resonance frequencies and ultimately the susceptibility. It should be possible to incorporate these considerations within the Green's-function formalism of Rezende and Hone.[17] The corresponding calculations for higher temperature and $\theta\neq0°$ have not yet been carried out.

The choice of a bulk FeF_2 crystal for our first investigation with a new instrument was partly because of the wealth of existing theory on the uniaxial antiferromagnets. We now plan to carry out studies on a range of other magnetic materials, both bulk and low dimensional, in which resonances in our spectral region are expected.

[1]R. E. Camley, Surf. Sci. Rep. 7, 103 (1987).

[2]D. R. Tilley, in *Linear and Nonlinear Spin Waves in Magnetic Films and Superlattices*, edited by M. G. Cottam (World Scientific, Singapore, 1994), Chap. 4.

[3]T. Dumelow, D. E. Brown, and T. J. Parker, in *18th International Conference on Infrared and Millimeter Waves*, Colchester, 1993, edited by James R. Birch and Terence J. Parker [Proc. SPIE 2104, 633 (1993)].

[4]R. C. Ohlmann and M. Tinkham, Phys. Rev. 123, 425 (1961).

[5]K. M. Häussler, A. Lehmeyer, and L. Merten, Phys. Status Solidi B 111, 513 (1982).

[6]K. M. Häussler, J. Brandmüller, L. Merten, H. Finsterhölzl, and A. Lehmeyer, Phys. Status. Solidi B 117, 225 (1983).

[7]L. Remer, B. Lüthi, H. Sauer, R. Geick, and R. E. Camley, Phys. Rev. Lett. 56, 2752 (1986).

[8]R. W. Sanders, R. M. Belanger, M. Motokawa, V. Jaccarino, and S. M. Rezende, Phys. Rev. B 23, 1190 (1981).

[9]A. M. Balbashov, G. V. Kozlov, S. P. Lebedov, A. A. Mukhin,

A. Yu. Pronin, and A. S. Prokhorov, Zh. Eksp. Teor. Fiz. **95**, 1092 (1989) [Sov. Phys. JETP **68**, 629 (1989)].

[10]A. A. Mukhin, A. Yu. Pronin, A. J. Prokhorov, G. V. Kozlov, V. Zeheny, and J. Petzelt, Phys. Lett. A **153**, 499 (1991).

[11]M. G. Cottam and D. J. Lockwood, *Light Scattering from Magnetic Systems* (Wiley, New York, 1986).

[12]T. Dumelow, T. J. Parker, S. R. P. Smith, and D. R. Tilley, Surf. Sci. Rep. **17**, 151 (1993).

[13]D. L. Mills and E. Burstein, Rep. Prog. Phys. **37**, 817 (1974).

[14]N. S. Almeida and D. L. Mills, Phys. Rev. B **37**, 3400 (1988).

[15]D. E. Brown, T. Dumelow, T. J. Parker, Kamsul Abraha, and D. R. Tilley, Phys. Rev. B **49**, 12 266 (1994).

[16]F. Keffer, in *Handbuch der Physik*, edited by S. Flügge

(Springer, Berlin, 1966), Vol. 18, Pt. II.

[17]S. M. Rezende and D. W. Hone, J. Phys. C **16**, 5899 (1983).

[18]R. Q. Scott and D. L. Mills, Phys. Rev. B **15**, 3545 (1977).

[19]G. W. Chantry, H. M. Evans, J. Chamberlain, and H. A. Gebbie, Infrared Phys. **9**, 85 (1969).

[20]J. Chamberlain, Infrared Phys. **11**, 25 (1971).

[21]J. Chamberlain and H. A. Gebbie, Infrared Phys. **11**, 56 (1971).

[22]W. G. Chambers, T. J. Parker, and A. E. Costley, in *Infrared and Millimeter Waves*, edited by K. J. Button (Academic, New York, 1986), Vol. 16, p. 77.

[23]N. S. Almeida (private communication).